Received: 3 July 2020 | Revised: 23 July 2020 | Accepted: 24 August 2020

DOI: 10.1049/hve2.12039

High Voltage

国家电网 STATE GRID 中国电力科学研究院有限公司 CHINA ELECTRIC POWER RESEARCH INSTITUTE | The Institution of Engineering and Technology | WILEY

ORIGINAL RESEARCH PAPER

Mobility-limited charge injection in cross-linked polyethylene under extra high electric field

Xi Zhu[1] | **Yi Yin**[1,2] | **Suman Peng**[1] | **Jiandong Wu**[1,2] | **Wenpeng Li**[3] | **Xin Chen**[3] | **Zhenyu Li**[4] | **Jianxin Guan**[4]

[1]Department of Electrical Engineering, School of Electronic Information and Electrical Engineering, Shanghai Jiao Tong University, Shanghai, China

[2]Key Laboratory of Control of Power Transmission and Conversion, Shanghai Jiao Tong University, Ministry of Education, Shanghai, China

[3]State Key Laboratory of Advanced Power Transmission Technology, Global Energy Interconnection Research Institute Corporation, Beijing, China

[4]State Grid of Corporation China, Beijing, China

Correspondence

Yi Yin, Shanghai Jiao Tong University, 800 Dongchuan Rd, Minhang District, Shanghai, China.
Email: yiny@sjtu.edu.cn

Associate Editor: Boxue Du

Funding information

National Key Research and Development Plan, Grant/Award Number: 2016YFB0900701; State Key Laboratory of Advanced Power Transmission Technology, Grant/Award Number: GEIRI-SKL-2019-007

Abstract

In this study, characteristics of charge injection under extra high electric field (above 100 kV/mm) in cross-linked polyethylene (XLPE) were investigated by experiments of conduction current and space charge. The results show that current density from low electric field to sample breakdown corresponds to space charge limited current (SCLC) theory. More specifically, Schottky current is similar to experiment current before 100 kV/mm, while the *J–E* curve conforms to a modified SCLC theory after 100 kV/mm. Besides, the non-linear coefficient of *J–E* curve from 100 kV/mm to extra high electric field is smaller than theoretical value, and the injection depth of space charge is restricted as the field becomes higher than 100 kV/mm, which may be caused by the negative differential mobility of charge. Driven by extra high electric field, charge collides with lattice of dielectric and scatters. As a result, mean free time of charge decreases and charge mobility is reduced with the increased field. Consequently, considering the decrease in charge mobility, a mobility-limited charge injection equation is proposed, and the validity of the proposed equation under extra high electric field is demonstrated by space charge simulation.

1 | INTRODUCTION

High-field conduction of polymer is different from the traditional Ohm's law, which has a significant non-linear volt–ampere characteristic. Research on the conduction characteristics of polymer could not only provide a theory basis for the design of the insulation structure, but also conduct a microcosmic investigation on charge transport, energy level distribution and trap density in dielectric [1]. Therefore, the research on high-field conduction of polymer is of great significance to explore the dielectric insulation performance and estimate the insulation life.

The non-linear conduction mechanism of polymers under high electric field mainly contains two types: electrode-limited model and bulk-limited model. The process in which charges overcome the work function of the metal electrode and inject into dielectric is the electrode-limited model, such as Schottky effect and the Fowler–Nordheim effect [2, 3]. And as the injection current becomes greater than the bulk conduction current in dielectric, charge accumulates in the interface between electrode and material, and the conduction mechanism turns into the bulk-limited model, such as Poole–Frankel effect, hopping conduction and space charge limited current (SCLC) theory [4–6]. As a commonly used insulation material for power cables, polyethylene has been widely studied for its non-linear conductivity characteristics under high electric fields. G. C. Montanari found that the current density of high-density polyethylene followed the typical Schottky law describing an injection-dominated conduction mechanism [7]. Researches by L. Lan showed that the conduction characteristics of cross-linked polyethylene (XLPE) under high electric field could be

explained by SCLC theory [8]. Besides, a research on carbon black/polyethylene composite found that the conduction characteristics under high fields were consistent with tunnelling effect [9], while a study found that the high-field conduction mechanism in silicon dioxide/low-density polyethylene composite was dominated by hopping conduction [5]. Although there have been a lot of researches on the high-field conduction of polyethylene, the test electric fields in previous studies were basically lower than 200 kV/mm. To ensure the safe operation of high-voltage electrical equipment under extra high electric field, it is of great significance to study the conduction mechanism of polyethylene before sample breakdown. Therefore, to reveal the high-field conduction at pre-breakdown in polymer, some researchers developed a novel measurement system for transient characterization of extreme field conduction [10], and the conductivities near breakdown were discussed by a simplified criterion for thermal breakdown [11], which allowed temperature dependent breakdown data to be converted to field-dependent breakdown data. These provide the necessary research foundation for study on polymer conductivity. But, how to eliminate the effect of material ageing on the conductivity characteristics in long-term high-field experiment is also needed for further study.

In addition, the current density of dielectric under high field is an important basis for the analysis of space charge injection in dielectrics. In the numerical calculation and simulation of space charge, the Neumann boundary for charge injection is usually chosen as Schottky equation [12, 13]. In parallel-plate electrode, a bipolar charge transport model based on Schottky injection, charge migration, trapping and recombination processes has been developed [14]. Furthermore, under higher electric field, Schottky equation was also applied to simulate the charge injection in needle-plate electrode [15, 16]. However, the correctness of choosing the Schottky equation as the injection equation under high fields has not been verified. Although T. Tanaka proposed that the tunnelling effects might occur at the needle tip [3], there is no clear experiment to verify this hypothesis. Therefore, studying the conductivity of polyethylene under extra high field and determining the charge injection equation, are of great significance for the further research on space charge characteristics under needle-plate electrodes.

In this study, samples of XLPE were prepared to investigate the conductivity characteristics of polyethylene from low electric field to sample breakdown. Space charge measurement and bipolar charge transport simulation were carried out to research the charge behaviour under extra high electric field. Furthermore, considering the variation in charge mobility, a mobility-limited charge injection equation was proposed to characterize the charge injection process under extra high electric field.

2 | EXPERIMENTAL PROCEDURES

2.1 | Sample preparation

XLPE samples used in this study were commercial-grade HVDC cable insulation materials. The XLPE pellets were mixed at 110°C for 5 min in a torque rheometer (RM-200C) to obtain a homogeneous material and eliminate possible pellet-to-pellet interfaces. Then, the material mixture was thermally pressed at 110°C at a pressure of 20 MPa and cross-linked at 180°C by a curing press. Finally, it was cooled naturally to room temperature under the mechanical pressure [8]. Plate samples with thickness of 20 μm were obtained for high-field conduction measurement and those with thickness of 150 μm were obtained for space charge measurement. Before test, the samples were all degassed at 70°C in vacuum (10^{-2} Pa) for 24 h to eliminate crosslinking by-products and avoid the mechanical stress.

2.2 | High-field conduction measurement

High-field conduction was conducted with Keithley 6517B, and the electrodes were designed according to IEC Standard [17], as shown in Figure 1. In order to study the semi-conduction-insulation-metal structure existing in practical engineering, the upper electrode is semi-conduction (SC) material and the lower electrode is aluminium. The conduction current was obtained by applying an initial electric field of 2 kV/mm and increasing the field in various increments to sample breakdown. Test temperature was maintained at 20°C. Although a long polarization time is beneficial to obtain the stable current value under high electric field, the long polarization time would cause the breakdown and ageing of the samples, which is not available to obtain the *J–E* curve from low to extra high electric field. Therefore, the polarization time was chosen as 300 s.

2.3 | Space charge measurement

Space charge distribution in sample was measured at 20°C by a pulsed electro-acoustic measurement system, as shown in Figure 2. The upper and lower electrode were SC and aluminium, respectively. The sample was polarized for 300 s at a series of positive DC electric fields and space charge distribution was acquired.

3 | RESULTS

3.1 | Current waveform before sample breakdown

Through a large number of experiments, it is found that the breakdown of XLPE sample generally occurs at 350 kV/mm. It is noted that the breakdown always suddenly occurred during the relaxation of current, as shown in Figure 3. The normal experiment result is shown by the solid black line, which is significantly consistent with the typical exponential decay trend. However, the sample would be broken down suddenly under high electric field, which could be divided into Case 1 and Case 2. The former is due to the breakdown in the measuring electrode, leading to the sudden increase of current, as shown in the dashed red line.

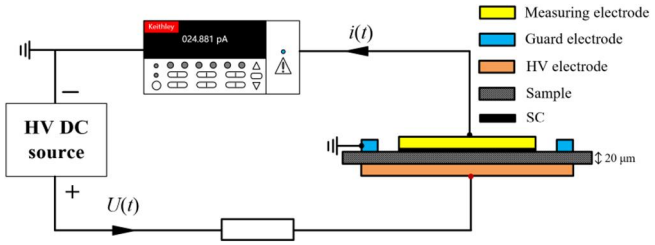

FIGURE 1 High-field conduction measuring apparatus

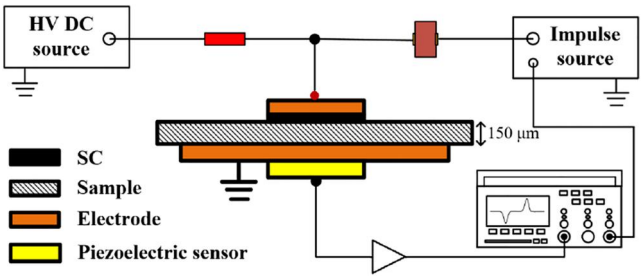

FIGURE 2 Pulsed electro-acoustic measurement system

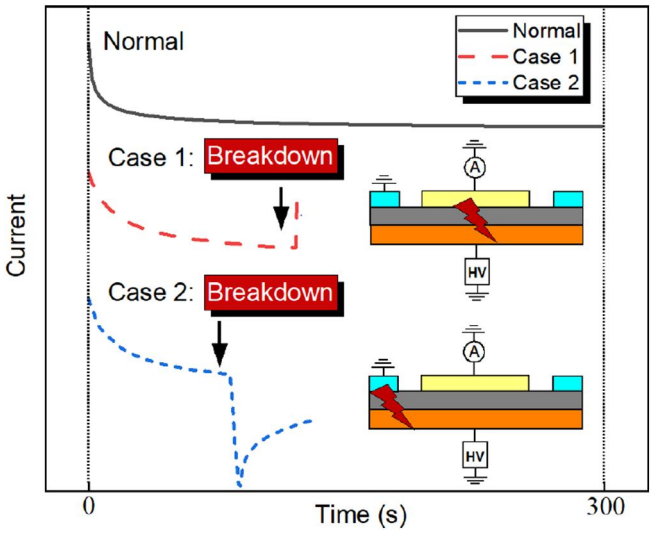

FIGURE 3 Current waveforms of breakdown

The latter is caused by the breakdown in the guard electrode, thus the measuring electrode is short-circuited and the current changes from polarization current to depolarization current, as shown in the dotted blue line. The current under the last electric field before the sample breakdown is recorded as the last data point.

Normally, the polarization current consists of steady conduction current and transient absorption current, where the polarization process includes fast charge current (relaxation time $\tau < 10^{-11}$ s) and slow current (10^{-2} s$<\tau <$ 104 s) [18]. Therefore, a two-phase exponential decay function is applied to fit the polarization current $I(t)$, excluding the transient absorption current and obtaining the steady conduction current I_0 as shown in Equation (1):

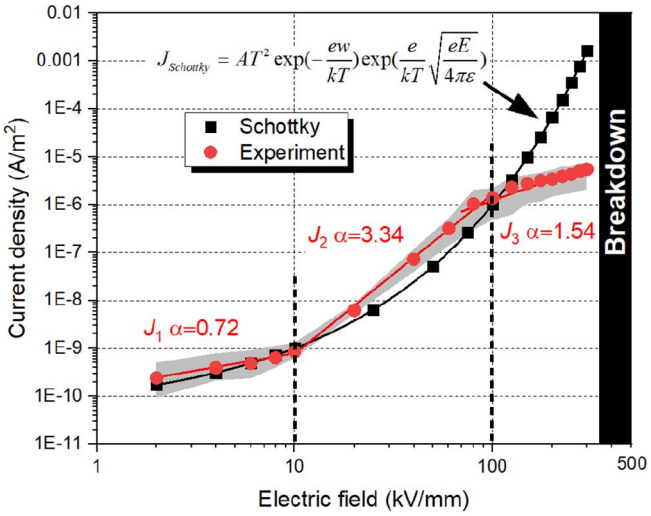

FIGURE 4 The relationship between current density and electric field

$$I(t) = I_0 + A_1 e^{-t/\tau_1} + A_2 e^{-t/\tau_2}. \quad (1)$$

where A_1 and τ_1 represent the fast polarization, A_2 and τ_2 represent the slow polarization, and the parameter I_0 is applied as the conduction current at each electric field.

3.2 | *J–E* curve

The current density under each electric field is shown in Figure 4, where the grey area is the maximum and minimum of the current data in three experiments. Meanwhile, the curve of Schottky current J_{Schottky} is calculated by Equation (2) and it is characterised in square black symbol.

$$J_{\text{Schottky}} = AT^2 \exp\left(-\frac{ew}{kT}\right)\exp\left(\frac{e}{kT}\sqrt{\frac{eE}{4\pi\varepsilon}}\right). \quad (2)$$

where e is elementary charge, ε is permittivity of the material and E is electric field, A is Richardson constant 1.2×10^6 A m^{-2} K^{-2}, k is Boltzmann constant 1.38×10^{-23} J K^{-1}, T is temperature 293 K, and the injection barrier of carriers w is set to 1.27 eV referring to previous studies [12].

It can be seen that the Schottky current increases significantly with electric field, while the current measured by experiment has three distinct regions with different slopes: (i) J_1: a slight increase at 2~10 kV/mm, (ii) J_2: a steep increase at 10~100 kV/mm, (iii) J_3: a slight increase at 100~350 kV/mm, which significantly corresponds to the SCLC theory [6]. Before 100 kV/mm, although there is a certain difference between the experimental data and Schottky current, the increase trend of experimental data is similar to that of Schottky current, and the currents of two curves are close in magnitude under each electric field. However, as the electric field reaches the extra high electric field (above 100 kV/mm), Schottky current

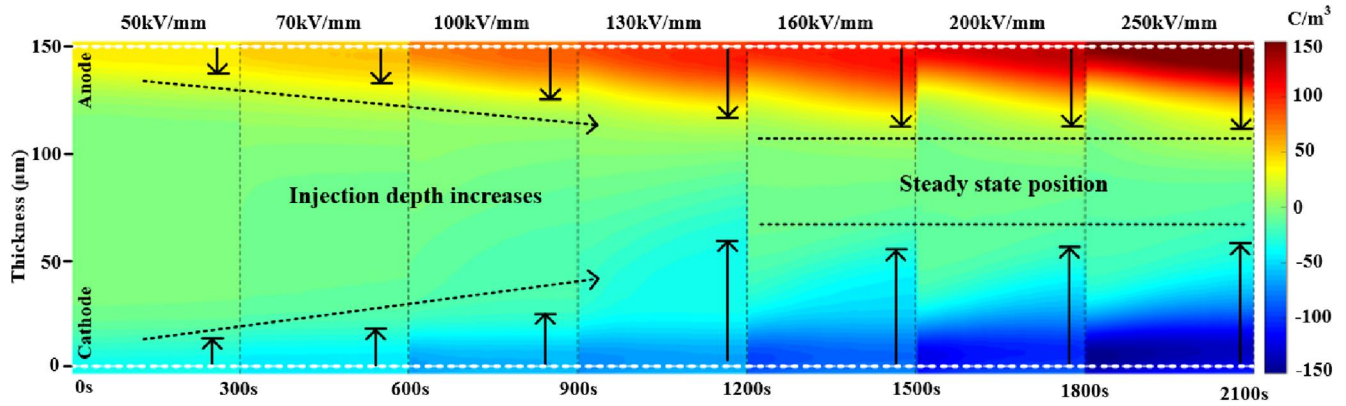

FIGURE 5 Spatial and temporal distribution of space charge

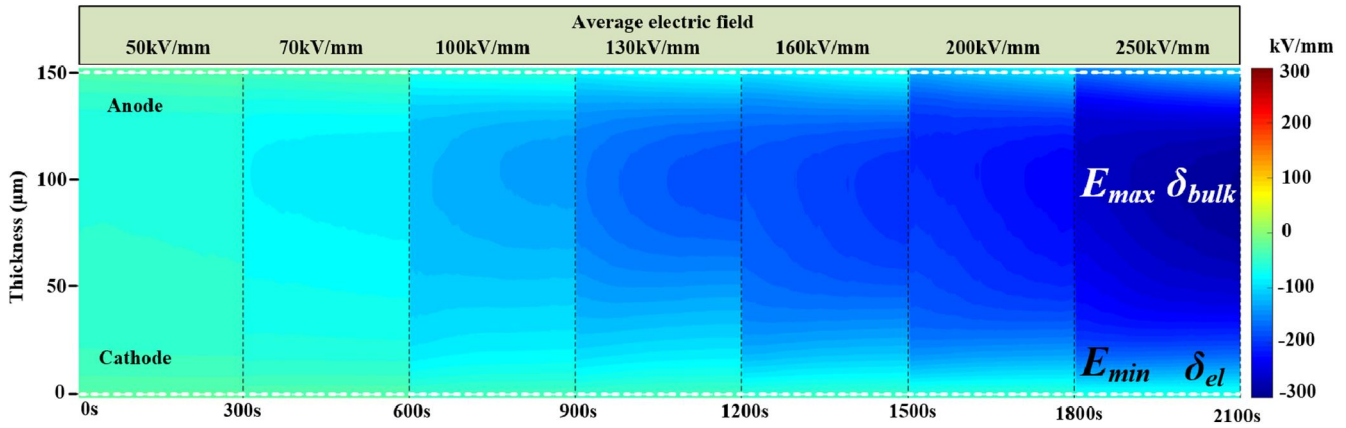

FIGURE 6 Spatial and temporal distribution of electric field

becomes much larger than experiment current. For example, the current density calculated by Schottky equation is one order of magnitude greater than that measured by experiment at 200 kV/mm; while as the field reaches 300 kV/mm, the Schottky current becomes three orders of magnitude greater than the experiment current.

A power law dependence of the *J*–*E* curve is expressed as:

$$J = K \cdot E^{\alpha}. \tag{3}$$

where K is the coefficient associated with material properties, and α is the non-linear coefficient. Through logarithmic transformation, the relationship can be derived as follows:

$$\lg J = \alpha \lg E + \lg K. \tag{4}$$

The relationship between current density J (A/m^2) and electric field E (kV/mm) is represented by a piecewise function (5):

$$\begin{cases} \lg J_1 = 0.72 \cdot \lg E - 3.82, & E \le 10 \\ \lg J_2 = 3.34 \cdot \lg E - 6.45, & 10 \le E \le 100 \\ \lg J_3 = 1.54 \cdot \lg E - 8.99, & 10\,0 \le E \end{cases}. \tag{5}$$

In general, the current calculated by Schottky equation is relatively close to the experiment result at the field lower than 100 kV/mm. However, the result of Schottky equation becomes much larger than experiment result at the field higher than 100 kV/mm. In XLPE, the application of SCLC theory to characterize the conductivity characteristics from low field to sample breakdown is reasonable and applicable.

3.3 | Space charge and electric field distribution

The space charge distribution of XLPE samples is illustrated through the colour map in Figure 5. The yellow and blue colours are applied to represent the positive and negative charge, respectively. The colour bar beside the data is applied to show the scale of the charge density for the colour map. The ordinate represents the position in the sample, where the anode and cathode positions are characterized by white lines. The abscissa represents the time and applied field. It can be found that the accumulation charge near the electrode is homo-charge and the charge density increases significantly with the increased electric field. Besides, negative charge is dominant and more widely distributed in XLPE than positive

charge, which agrees with other scholars' researches [8, 19]. Although some studies reported that the positive charge injection happened more easily [20], the different results of space charge may be caused by the different charge transport and injection characteristics in diverse polythene materials. Moreover, it should be noted that, due to the limitation of the colour resolution of colour map, the less space charge inside the material could not be distinguished clearly when there is a large amount of charge around electrodes. But in fact, charge transports deeper to the middle of the sample and even the positive and negative charges are in contact with each other at the field larger than 100 kV/mm.

Furthermore, the electric field distribution in the sample is shown in Figure 6. It can be seen that the electric field in the material is significantly distorted, where the field inside the sample is enhanced and the field near the electrode is weakened. The distortion rate δ of electric field is applied to characterize the changing of electric field as follows [21]:

$$\delta_{\text{bulk}} = \frac{E_{\max} - E_{\text{av}}}{E_{\text{av}}} \qquad \delta_{\text{el}} = \frac{E_{\text{av}} - E_{\min}}{E_{\text{av}}}. \tag{6}$$

where the $E_{\max}$ is the maximum value of electric field inside the sample, $E_{\min}$ is the minimum value of electric field near the electrode and E_{av} is the ideal average electric field. Due to the significant injection of electron in cathode, the δ_{el} near cathode and δ_{bulk} inside the material are shown in Table 1.

It can be seen that δ_{bulk} increases first and then decreases with the increased electric field, by contrast, the δ_{el} increases with the increased electric field and it reaches an approximate steady state. There is a noteworthy phenomenon, as the electric field is lower than 100 kV/mm, δ_{bulk} is larger than δ_{el}. However, as the field becomes larger than 130 kV/mm, the δ_{bulk} becomes smaller than δ_{el}. It indicates that the shielding effect of charge around electrode becomes significant under high electric field, by contrast the enhancing effect of charge inside the sample is restricted. Furthermore, considering the dependent of δ_{el} on average electric field E_{av}, an exponential attenuation model is applied to estimate the variation of δ_{el}:

$$\delta_{\text{el}} = p_1 + p_2 \exp(p_3 E_{\text{av}}). \tag{7}$$

The fitting result is shown in Figure 7. R-square (≈0.986) indicates that the exponential attenuation model can effectively characterize the relationship between δ_{el} and E_{av}.

3.4 | Charge mobility under different electric fields

Based on the space charge distribution shown in Figure 5, it can be seen that the charge gradually migrates into the sample with time, but the charge injection depth at 300 s under different electric fields has a particular phenomenon as described in Figure 8, where the injection depth of charge reaches a steady state with the increased electric field. As the electric field is lower than 100 kV/mm, the injection depth of charge at 300 s, whether positive or negative, increases with the increased field. However, the charge injection depth is restricted at the electric field higher than 100 kV/mm, and it seems to reach a steady state, such as 80 μm for negative charge and 45 μm for positive charge. It is noted that there is a high injection depth of the negative charge under 130 kV/mm, which may be caused by the more significant recombination of negative and positive charge under higher electric field. Therefore, the corresponding velocity v of charge would also reach a steady state, which could be calculated by dividing the injection depth by the time [22, 23]. However, the mobility would decrease with the increased electric field referring to Equation (8)

$$v = \mu E. \tag{8}$$

where μ is charge mobility. Based on the results of charge injection depth, the mobility of positive and negative charge under different electric fields is shown in Table 2. It can be seen that the mobility of charge decreases significantly with the increased electric field. Moreover, the mobility of negative charge is larger than that of positive charge. The calculated mobility in this article agrees with other researches based on isothermal depolarization current and surface potential decay measurement [24,

TABLE 1 Distortion rate δ under different electric fields

E_{av} (kV/mm)	$E_{\max}$ (kV/mm)	δ_{bulk} (%)	$E_{\min}$ (kV/mm)	δ_{el} (%)
50	58.9	17.8	43.6	12.9
70	86.4	23.5	55.4	20.9
100	126.9	26.8	72.7	27.3
130	187.6	44.3	89.5	31.2
160	204.7	28.0	112.0	30.0
200	231.7	15.8	133.6	33.2
250	294.2	17.7	170.5	31.8

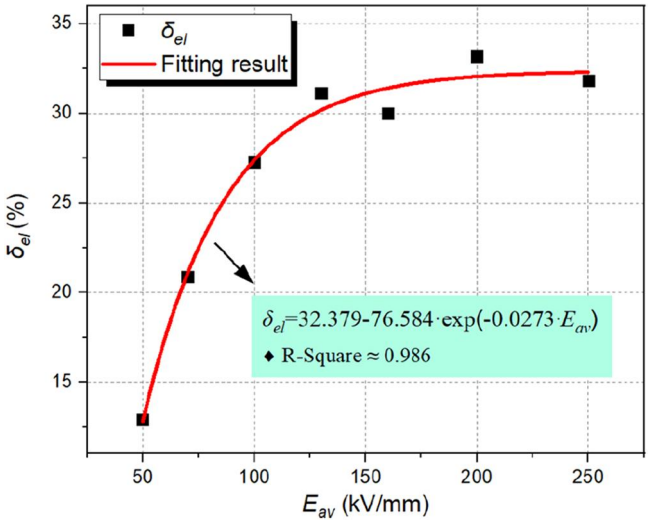

FIGURE 7 Fitting results of δ_{el} under different E_{av}

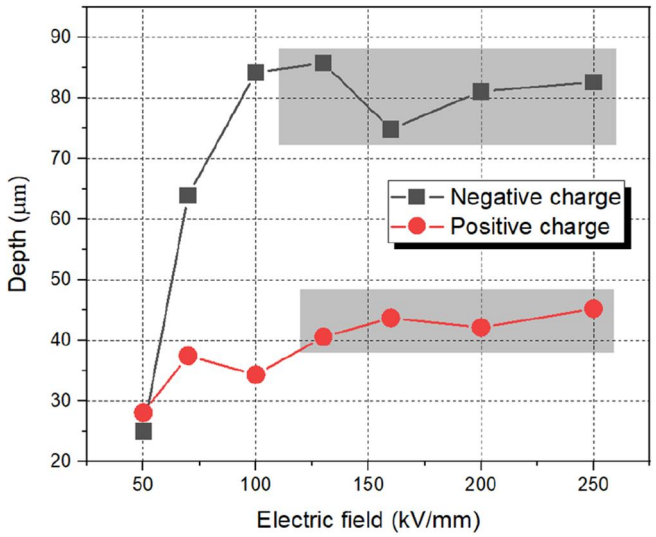

FIGURE 8 Injection depths of charge under different electric fields

TABLE 2 Charge mobility under different electric fields

	Mobility ($\times 10^{-15}$ $m^2 \cdot V^{-1} s^{-1}$)	
E_{av} (kV/mm)	Negative charge	Positive charge
100	2.81	1.14
130	2.20	1.04
160	1.56	0.91
200	1.35	0.70
250	1.10	0.60

25], demonstrating the validity of the charge mobility in magnitude. Furthermore, the exponential function is suitable for fitting the decrease in mobility of positive and negative charge under different electric fields, as shown in Figure 9.

4 | DISCUSSION

4.1 | Conduction mechanism in XLPE from low to high electric field

The current density in experiment from low electric field to sample breakdown has two threshold electric fields (10 kV/mm and 100 kV/mm) and three distinct regions with different slopes. The characteristics of conduction current under different electric fields are discussed in detail.

i. As the field is lower than 10 kV/mm, the charge injection is little, and the current density obeys the Ohm law, which could be expressed as Equation (9)

$$J = e\mu nE. \tag{9}$$

where e is elementary charge, n is charge density.

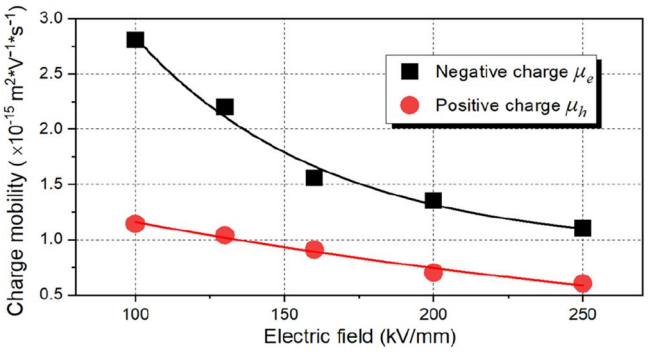

FIGURE 9 Dependence of charge mobility on electric field

ii. As the field increases from 10 kV/mm to 100 kV/mm, charge is injected and captured by traps. Moreover, from the *J–E* curve shown in Figure 4, the experiment current is close to the Schottky current. The conduction characteristic may be associated with Schottky emission and SCLC theory

First of all, the electrode-limited current, Schottky current, is illustrated in Figure 10a. The work function of metal is Φ_D, and the actual barrier $\Phi_0(x)$ is the electrostatic attraction between electrons and induced positive charges in metal surfaces. Under the electric field, the final barrier $\Phi(x)$ is expressed as follows:

$$\Phi(x) = \Phi_0(x) - eEx = -\frac{e^2}{16\pi\varepsilon x} - eEx. \tag{10}$$

The highest barrier Φ_{max} and the position of the highest barrier x_{max} could be calculated as follows:

$$\Phi_{max} = -\sqrt{\frac{e^3E}{4\pi\varepsilon}}; \quad x_{max} = \sqrt{\frac{e}{16\pi\varepsilon E}}. \tag{11}$$

As shown in Figure 10a, the injection barrier moves to the lower left with the increased electric field, decreasing Φ_{max} and x_{max}. As a result, there is a lower and thinner injection barrier for Schottky injection, which enhances the charge injection from electrode and accounts for the injection current.

And then, the bulk-limited current, SCLC, is illustrated in Figure 10b. There is a basic requirement in SCLC model: the electrode must take ohmic contact to the insulator to ensure the sufficient space charge in the dielectric [6]. But, due to the lower and thinner injection barrier under high electric field, a large amount of charge would be injected by Schottky emission. Therefore, although the electrode and insulator are not in ohmic contact, the sufficient injected charge and the trapping process make the conduction characteristic of the dielectric conform to the SCLC model. As shown in Figure 10b, the injection current J_i becomes larger than the electron current J_e in dielectric, which leads to the homo-charge accumulation near the electrode. The existence of space charge causes the SCLC J_s, leading to $J_i = J_e + J_s$. Due to $J_s >> J_e$, the SCLC

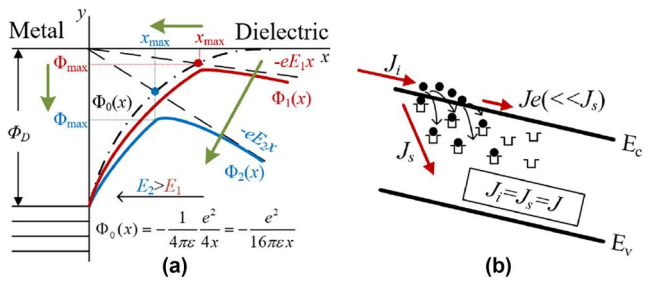

FIGURE 10 Space charge injection and formation of conduction current. (a) Electron injection by Schottky emission, (b) space charge limited current in dielectric

accounts for the conduction current in dielectric. It is noted that different distribution of trap level accounts for different trap-limited SCLC. For example, evenly distributed trap levels lead to the SCLC where non-linear coefficient α equals to 1; traps limited to single and multiple discrete energy levels would cause α close to 2. Besides, in the exponentially distributed trap levels, trap-limited SCLC could be expressed as follows [6]:

$$J = N_0 \mu e^{1-l} \left[\frac{\epsilon l}{H(l+1)}\right] \left(\frac{2l+1}{l+1}\right)^{l+1} \frac{V^{l+1}}{d^{2l+1}}. \quad (12)$$

where N_0 is effective state density in valence band, H is the total trap density, d is sample thickness. According to the results shown in function Equation (5), α of J_2 is about 3 and l approximately equals to 2, demonstrating the trap-limited SCLC where the trap energy level is exponentially distributed.

In general, from 10 to 100 kV/mm, the Schottky current is promoted due to the lower and thinner injection barrier. Meanwhile, a large amount of injected charge accumulates in dielectric, making the conduction characteristic of the dielectric conform to SCLC model as well.

i. As the electric field further increases (larger than 100 kV/mm) until the sample breakdown, the number of charges would be more than that of traps, which may lead to the traps to be completely filled by charges. The trap-free SCLC current is shown as the Child law [6]

$$J = \frac{9}{8}\mu\epsilon\frac{V^2}{d^3}. \quad (13)$$

But, it is noted that the non-linear coefficient α of J_3 is about 1.54 according to the experiment results, which is relatively smaller than the theoretical value ($\alpha = 2$) in Equation (13). The decrease in α may be caused by the decrease of mobility under extra high electric field, which would be further discussed in the following section. Besides, the Schottky equation is no longer applicable to characterize charge injection under extra high field in XLPE, and a proper electrode-limited injection equation is needed.

In summary, as the electric field is lower than 100 kV/mm, the conduction process of XLPE commonly consists of electrode-limited conduction and bulk-limited conduction. But, as the electric field reaches an extra high value, the bulk-limited conduction would be changed and the electrode-limited conduction has not been clarified.

4.2 | Negative differential mobility under extra high electric field

According to the experiment results of charge mobility shown in Table 2, it can be seen that charge mobility decreases significantly with the increased electric field. It is speculated that the smaller non-linear coefficient of *J–E* curve at the field larger than 100 kV/mm is due to the decrease in charge mobility under extra high electric field.

There have been some studies on the negative differential mobility of charge, which can be roughly divided into two aspects. (i) In semiconductor materials, the charge mobility decreases with the increased electric field when the temperature T exceeds a reference temperature T^*. Besides, Gunn effect in gallium arsenide is also applied to account for the decrease in charge velocity [26]. (ii) In the polymer insulation, the morphology of polyethylene changes with electric field, which weakens the tunnelling process and consequently reduces charge mobility. Also, the formation of charge packet in materials may be an un-negligible factor for the negative differential mobility [23]. However, the test electric field in previous studies is low (<150 kV/mm) and few performed at pre-breakdown. Thus, the effect of impact ionization before sample breakdown may be available to reveal the negative differential mobility.

The possible impact ionization of charge would occur as shown in Figure 11. Driven by electric field, carriers acquire energy, and the energy transfers to the lattice of dielectric by collision. Under a low electric field, the energy released from collision equals the lattice energy. And the thermal velocity v_t is much larger than drift velocity v_d, thus mean free time τ between collisions is a constant as shown in Equation (14) [26]:

$$\tau = \frac{l}{v_d + v_t} \approx \frac{l}{v_t}. \quad (14)$$

where l is the mean free distance between collisions. But, under extra high electric field, the extended state in dielectric becomes wider and the energy of carriers would be higher than that of lattice. Thus, the drift velocity increases with the increased electric field as follows:

$$v_d = \mu E. \quad (15)$$

Consequently, v_d becomes larger than v_t, and τ becomes a function of v_d as shown in Equation (16):

$$\tau = \frac{l}{v_d + v_t} \approx \frac{l}{v_d}. \quad (16)$$

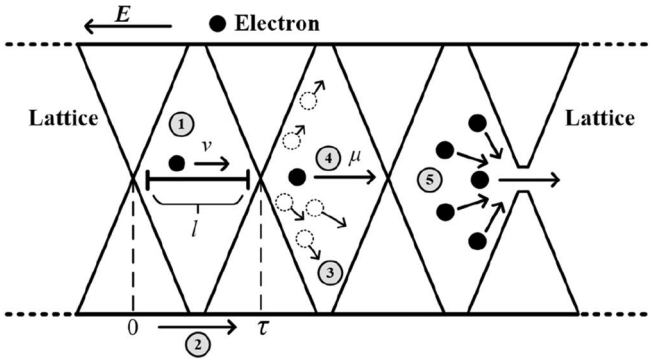

FIGURE 11 Reaction between charge and lattice. (a) Charge migration as velocity of v between collisions with distance of l, (b) mean free time τ between collisions, (c) charge scattering after collision, (d) decreasing in mobility of charge, (e) broken lattice after multiple collisions

It can be seen that as the electric field increases, v_d increases, consequently reducing τ. Considering the scattering effect of electrons after collision, the mobility is expressed as follows:

$$\mu = \frac{e\tau}{m^*}. \tag{17}$$

where m^* is effective mass. Thus, due to the scattering of high-energy charge after collision with lattice, the mean free time decreases and as a result the mobility is reduced with the increased electric field. Furthermore, due to the multiple collisions by charges, the lattice structure of dielectric would be destroyed and the sample breakdown occurs.

In summary, the collisions of charges with lattice and charge scattering after collisions may be critical factors to the decrease in mobility and sample breakdown, reducing the nonlinear coefficient of *J–E* curve in XLPE from 100 kV/mm to extra high electric field.

4.3 | Mobility-limited charge injection equation under extra high electric field

Under the premise that the conduction current in sample bulk and the injection current in electrode are continuous, the charge injection equation under extra high electric field is discussed as follows.

Based on the relationship between δ_{el} and E_{av} shown in Figure 7, the actual electric field in cathode E_{el} under different E_{av} is calculated in Table 3, and the corresponding current density obtained by experiment is shown in Figure 12. In general, charge would be injected into samples from electrodes by tunnelling process as the electric field becomes larger than 100 kV/mm, which is expressed as Fowler–Nordheim effect as shown in Figure 12. The Fowler–Nordheim equation is applied to fit the current density J with E_{el}. R-square (≈0.996) seems to indicate that the experimental data fit the equation well, but the fitting result of parameter B contains a minus sign ($B = -141.85$), which demonstrates the unavailability of the equation in describing the charge injection in XLPE under extra high electric field.

It is noted that, because parameter B is a negative number, the effect of the exponential term in Fowler–Nordheim equation on current changes from promotion to suppression as the electric field increases. Considering the continuity between electrode-limited current and bulk-limited current, the negative differential mobility of charge in dielectric bulk may account for the weakening of charge injection from electrode under extra high electric field. A large amount of charge is injected into dielectric with the increased electric field, but the saturation of charge velocity may restrict the charge migration into dielectric. As a result, there is a lot of homo-charge accumulating around the electrode, which would increase the injection barrier and weaken the electric field inevitably. The shielding effect of charge on electrode becomes significant while the enhancing effect of charge on electric field inside the sample is restricted. Therefore, the charge injection process under extra high electric field no longer follows the Schottky law or Fowler–Nordheim law. By contrast, a mobility-limited charge injection equation considering the decrease of mobility in dielectric bulk is proposed as Equation (18). Moreover, considering the possible effect of temperature on conduction characteristics [8, 27], some parameters in Equation (18) are set as a function of temperature:

$$J_{m-l} = A(T) \cdot E^2 \exp(B(T)/E). \tag{18}$$

where $A(T)$ is associated with injection barrier and temperature, $B(T)$ is associated with the effect of the negative differential mobility and temperature. Although Equation (18) is similar in form to the Fowler–Nordheim equation, the sign of the B reflects different charge injection mechanisms, and the fitting result in Figure 12 also demonstrates the validity of Equation (18). But, it is noted that the fitting result is developed based on the experiments at 20°C. In our later studies, the effect of temperature on the conduction characteristics under extra high electric field would be further investigated to define the expression of $A(T)$ and $B(T)$.

In general, through research on *J–E* curve and space charge results from low electric field to extra high electric field, the mechanism of charge injection and migration in XLPE is summarized as Table 4.

4.4 | Simulation of space charge based on the mobility-limited charge injection equation

From discussions above, the mobility-limited charge injection equation is proposed to replace Schottky equation under extra high electric field. To further verify the validity of mobility-limited charge injection equation, a space simulation is carried out, where the size of simulation model is the same as that in space charge experiment. And the electric field in simulation is 250 kV/mm.

TABLE 3 Calculated δ_{el} and E_{el} under different E_{av}

	E_{av} (kV/mm)						
Results	**150**	**175**	**200**	**225**	**250**	**275**	**300**
δ_{el} (%)	31.10	31.73	32.05	32.21	32.30	32.34	32.36
E_{el} (kV/mm)	103.3	119.5	135.9	152.5	169.3	186.1	202.9

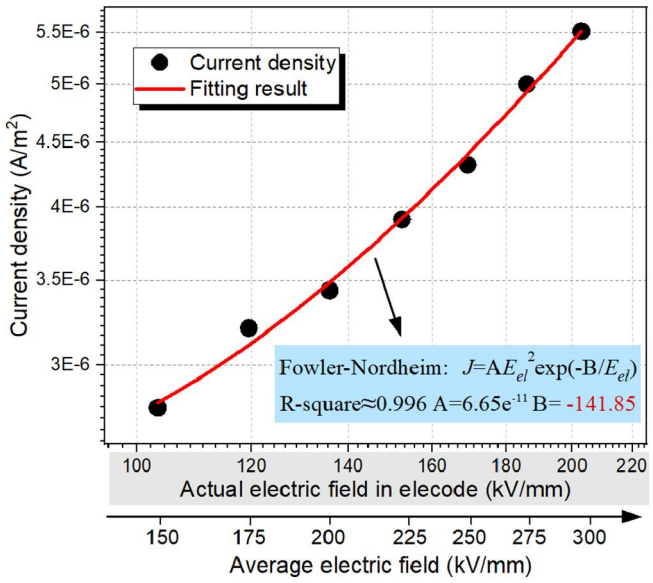

FIGURE 12 Current density with actual electric field

Firstly, the modified charge injection equation consists of Equation (2) at field lower than 100 kV/mm and Equation (18) at field higher than 100 kV/mm, is shown in Equation (19):

$$J_{\text{injection}} = \begin{cases} J_{\text{Schottky}}(E) & E \le 100 \text{ kV/mm} \\ J_{m-l}(E) & E > 100 \text{ kV/mm} \end{cases}. \tag{19}$$

and then, the charge transport function is described as:

$$j(x,t) = \mu(E)n(x,t)E(x,t) - D_f(\mu)\frac{dn(x,t)}{dx}. \tag{20}$$

where $\mu(E)$ represents the dependence of mobility on electric field, and $D_f(\mu)$ represents the diffusion coefficient considering a comparable Einstein equation as:

$$D_f(\mu) = \mu(E) \cdot T. \tag{21}$$

Based on the results in Figure 9, the dependence of charge mobility on electric field is applied in the simulation, and the corresponding diffusion coefficient of charge is also calculated through Equation (21).

Besides, charge trapping, de-trapping, recombination and extraction processes are also considered, which is illustrated in Figure 13. It can be seen that space charge distribution significantly affects the electric field distribution according to Poisson's equation, further changing the charge injection, transport and extraction processes. Besides, some parameters independent on space charge are shown in Table 5 [12–14].

To quantify the degree of the charge accumulation, the mean charge density q_{mean} in the sample is calculated mathematically as follows [28]:

$$\rho_{\text{acc}}(x,t) = \rho_{\text{app}}(x,t) - \frac{V_{\text{app}}}{V_{\text{ref}}}\rho_{\text{ref}}(x,t). \tag{22}$$

$$q_{\text{mean}}(t) = \frac{1}{d}\int_{x_0-d}^{x_0} |\rho_{\text{acc}}(x,t)| \, dx. \tag{23}$$

where V_{app} represents the applied voltage, V_{ref} represents the reference voltage, ρ_{app} represents the charge distribution at applied voltage, ρ_{ref} represents the charge distribution at reference voltage, ρ_{acc} represents the true charge distribution, x_0 is the anode position, and d is the thickness of the sample.

Three simulations are developed as shown in the Table 6, where Schottky equation is applied in simulation I but the modified injection equation is applied in simulation II and III. Moreover, to reveal the effect of charge migration on charge accumulation, the mobility and diffusion coefficient in simulation II is dependent on the electric field as shown in Figure 9, by contrast, those in simulation III are set as constants which are the values at 250 kV/mm.

The simulation results of q_{mean} at different times are calculated and shown in Figure 14. It can be seen that q_{mean} in simulation I is larger than that obtained by experiment, whereas q_{mean} in simulation II is close to that obtained by experiment. Moreover, by comparing simulation II and simulation III, it can be seen that the simulation result with negative differential mobility is closer to the experimental result than that with constant mobility. It is noted that the difference between simulation I and simulation II decreases with the increased time, which may be caused by the transient distributing of space charge.

In general, the modified injection equation, consists of Schottky equation and mobility-limited charge injection equation, is available to characterise the space charge injection in XLPE. And, the negative differential mobility of charge is also demonstrated to better characterize the space charge accumulation in XLPE under extra high electric field.

Furthermore, from discussion above, space charge injection and impact ionization are key points for the breakdown of XLPE. At present, addition of nano-filler is suitable for improving the dielectric insulation properties, such as less charge accumulation and higher breakdown strength [29]. Besides, voltage stabilizers, as additives in polyethylene, could more easily combine with high-energy electrons under electric field, weakening the collision of electrons on the dielectric lattice. Even voltage stabilizers can transfer electrons to any ionized molecular chains, preventing the free radical chain reactions and promoting the electrical insulation properties of polyethylene [30]. Therefore, material modification in fabrication or manufacture techniques is an effective way to improve the reliability of electrical insulation, which is of great significance for the development of polyethylene insulation materials.

TABLE 4 Mechanism of charge injection and migration from low electric field to extra high electric field

Description	Field range	Electrode-limited current	Bulk-limited current	Notes
Low	0~10 kV/mm	None	Ohm law: $J = e\mu nE$	None
High	10~100 kV/mm	Schottky injection: $J_{\text{Schottky}} = AT^2 \exp\left(-\frac{e\varphi}{kT}\right)\exp\left(\frac{e}{kT}\sqrt{\frac{eE}{4\pi\varepsilon}}\right)$	SCLC theory: $J = N_0\mu e^{1-l}\left[\frac{el}{H(l+1)}\right]\left(\frac{2l+1}{l+1}\right)^{l+1}\frac{V^{l+1}}{d^{2l+1}}$	Combined effect of charge injection and charge trapping
Extra high	100 kV/mm to breakdown	Mobility-limited charge injection: $J_{m-l} = A(T)E^2\exp(B(T)/E)$	SCLC theory: $J = \frac{9}{8}\varepsilon\frac{V^2}{d^3}\cdot\mu(E)$	Negative differential mobility of charge due to charge collision with lattice

Abbreviation: SCLC, space charge limited current.

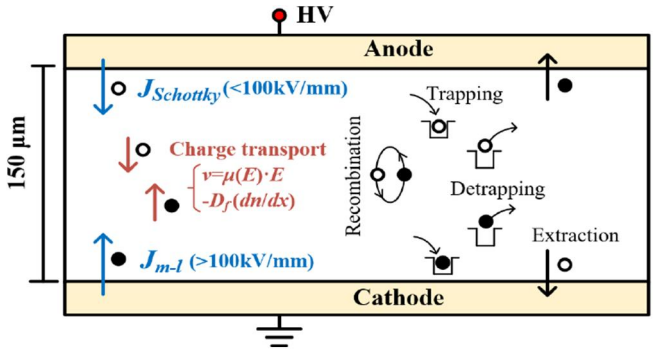

FIGURE 13 Bipolar charge transport model in simulation

TABLE 5 Specific simulation parameters of XLPE

Parameters	Description	XLPE	Unit
$B_e = B_h$	Trapping coefficient	0.1	s^{-1}
$S_0 = S_1 = S_2$	Recombination coefficient	4×10^{-3}	$m^3 \cdot C^{-1} \cdot s^{-1}$
S_3	Recombination coefficient	0	$m^3 \cdot C^{-1} \cdot s^{-1}$
$C_h = C_e$	Extraction coefficient	0.8	1
ΔU_{dtr}	Trap depth	0.9	eV
ε_r	Relative permittivity	2.3	1
T	Temperature	293	K

Abbreviation: XLPE, cross-linked polyethylene.

TABLE 6 Three simulations with different parameters

Number	Injection equation	Mobility	Diffusion coefficient
I	Equation (2)	$\mu(E)$	$D_f(\mu)$
II	Equation (19)	$\mu(E)$	$D_f(\mu)$
III	Equation (19)	μ(250 kV/mm)	D_f(250 kV/mm)

5 | CONCLUSION

In this study, samples of XLPE were prepared to investigate the characteristics of conductivity from low electric field to extra high electric field (above 100 kV/mm). Moreover, space charge experiment and simulation were developed respectively to research the charge injection and migration processes. The main conclusions are as follows:

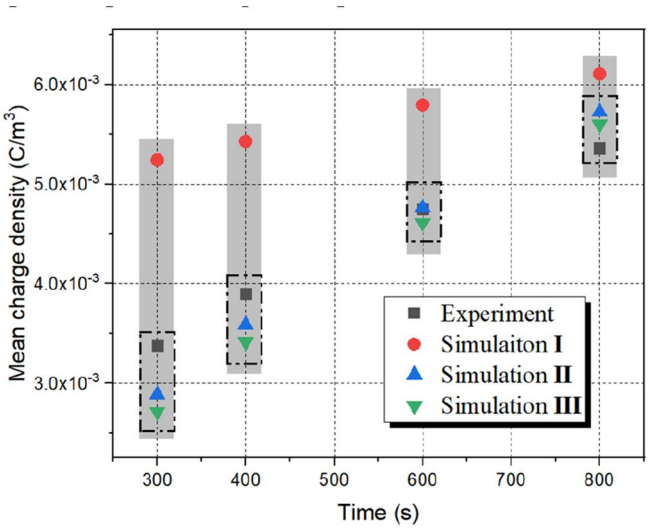

FIGURE 14 Mean charge density in experiment and simulation

i. The current density in XLPE from low electric field to extra high electric field corresponds to the SCLC theory. More specifically, the Schottky current is similar to experiment current at the field lower than 100 kV/mm, which may be caused by the combined effect of charge injection and charge trapping process. However, as the electric field becomes higher than 100 kV/mm, the Schottky emission is no longer applicable to characterize charge injection, and the *J–E* curve conforms to a modified SCLC theory
ii. Non-linear coefficient of *J–E* curve from 100 kV/mm to extra high electric field is relative smaller than the theoretical value. And, the injection depth of space charge is restricted as the electric field becomes higher than 100 kV/mm. These may be caused by the negative differential mobility of charge under extra high electric field in XLPE. Due to the collisions of charges with lattice of dielectric and the charge scattering after collisions under extra high electric field, the mean free time of charge decreases and the charge mobility is reduced. Furthermore, the lattice structure would be destroyed by multiple collisions, resulting in the sample breakdown
iii. Schottky effect and Fowler–Nordheim effect are not acceptable to denote the injection current under extra high

electric field. By contrast, a mobility-limited charge injection equation considering the decrease of charge mobility in dielectric bulk is proposed, which is available to characterise the charge injection process under extra high electric field in XLPE. A space charge simulation based on the bipolar charge transport model has demonstrated the validity of the proposed equation and the negative differential mobility, which may provide a basis for the charge simulation under concentrated electric field

ACKNOWLEDGEMENTS

This work is supported by the National Key Research and Development Plan (2016YFB0900701) and the State Key Laboratory of Advanced Power Transmission Technology (grant no. GEIRI-SKL-2019-007).

REFERENCES

1. Wang, X., Nelson, J. K., Schadler, L. S., et al.: Mechanisms leading to nonlinear electrical response of a nano p-SiC/silicone rubber composite. IEEE Trans. Dielectr. Electr. Insul. 17(6), 1687–1696 (2010)
2. Walker, A., Kambili, A., Martin, S.: Electrical transport modelling in organic electroluminescent devices. J. Phys. Condens. Matter. 14(42), 9825–9876 (2002)
3. Tanaka, T., Greenwood, A.: Effects of charge injection and extraction on tree initiation in polyethylene. IEEE Trans. Power App. Syst. PAS-97(5), 1749–1759 (1978)
4. Furlan, J., Gorup, Z., Levstek A., et al.: Thermally assisted tunneling and the Poole-Frenkel effect in homogeneous a-Si. J. Appl. Phys. 94(12), 7604–7610 (2003)
5. Yin, Y., Chen, J., Li, Z., et al.: High field conduction of the composites of low-density polyethylene/nano SiOx and low-density polyethylene/micrometer SiO2. Paper presented at International Symposium on Electrical Insulating Materials, Kitakyushu, Japan, June 2005, pp. 405–408
6. Mark, P., Helfrich, W.: Space-charge-limited currents in organic crystals. J. Appl. Phys. 33(1), 205–215 (1960)
7. Montanari, G. C., Mazzanti, G., Palmieri, F., et al.: Space-charge trapping and conduction in LDPE, HDPE and XLPE. J. Phys. Appl. Phys. 34(18), 2902–2911 (2001)
8. Lan, L., Wu, J., Yin, Y., et al.: Effect of temperature on space charge trapping and conduction in cross-linked polyethylene. IEEE Trans. Dielectr. Electr. Insul. 21(4), 1784–1791 (2014)
9. Xi, B., Chen, G.: The mechanism of electrical conduction in polyethylene/carbon black composite. In Proceedings of the IEEE International Conference on Properties and Applications of Dielectric Materials, Xi'an, China, June 2000, pp. 1015–1018
10. Li, Z., Xu, C., Uehara, H., et al.: Transient characterization of extreme field conduction in dielectrics. AIP Adv. 6(11), 115025 (2016)
11. Ho, J., Richard, T.: High field conduction in biaxially oriented polypropylene at elevated temperature. IEEE Trans. Dielectr. Electr. Insul. 19(3), 990–995 (2012)
12. Taleb, M., Teyssedre, G., Roy, S. L., et al.: Modeling of charge injection and extraction in a metal/polymer interface through an exponential distribution of surface states. IEEE Trans. Dielectr. Electr. Insul. 20(1), 311–320 (2013)
13. Liang, H., Du, B., Li, J., et al: Improved space charge transport model in bilayer dielectrics—considering carrier dynamic equilibrium. High Volt. 5(2), 176–183 (2020)
14. Alison, J., Hill, R.: A model for bipolar charge transport, trapping and recombination in degassed crosslinked polyethene. J. Appl. Phys. 27(6), 1291–1299 (1999)
15. Zhu, X., Wu, J., Wang, Y., et al.: Characteristics of electrical tree defect during the growth period in high-voltage DC cable under stepped DC voltage', IET Generation. Transm. Distrib. 13(15), 3195–3201 (2019)
16. Zhang, Y., Zhou, Y., Wu, C., et al.: Charge transport dynamics and the effects on electrical tree degradation under DC voltages in thermally aged silicone rubber, J. Phys. Appl. Phys. 53(41), 415501 (2020). https://doi.org/10.1088/1361-6463/ab876b
17. IEC 60093: Methods of Test for Volume Resistivity and Surface Resistivity of Solid Electrical Insulating Materials. International Electrotechnical Commission, Geneva (1980)
18. Beigert, M., Kranz, H.: Destruction free ageing diagnosis of power cable insulation using the isothermal relaxation current analysis. Proceedings of IEEE International Symposium on Electrical Insulation, Pittsburgh, USA, June 1994, pp. 17–21
19. Teyssedre, G., Laurent, C., Montanari, G., et al.: Charge distribution and electroluminescence in cross-linked polyethylene under dc field. J. Phys. Appl. Phys. 34(18), 2830–2844 (2001)
20. Matsui, K., Tanaka, Y., Takada, T., et al.: Space charge behavior in low density polyethylene at pre-breakdown. IEEE Trans. Dielectr. Electr. Insul. 12(3), 406–415 (2005)
21. Dai, C., Yin Y., Zhou, G., et al.: Space charge behavior in ethylene propylene rubber under a 50-Hz AC electric field. IEEE access, 7, 171995–172003 (2019)
22. Jones, J., Llewellyn, J., Lewis, T.: The contribution of field-induced morphological change to the electrical aging and breakdown of polyethylene. IEEE Trans. Dielectr. Electr. Insul. 12(5), 951–966 (2005)
23. Chen, G., Zhao, J.: Observation of negative differential mobility and charge packet in polyethylene. J. Phys. Appl. Phys. 44(21), 212001 (2011)
24. Mazzanti, G., Montanari, G., Alison, J.: A space-charge based method for the estimation of apparent mobility and trap depth as markers for insulation degradation-theoretical basis and experimental validation. IEEE Trans. Dielectr. Electr. Insul. 8(2), 187–197 (2008)
25. Matallana, J., Bigarre, J., Hourquebie, P., et al.: Recent experiments on space charge and transport in polyethylene under high DC field. Proceedings of Annual Report Conference on Electrical Insulation and Dielectric Phenomena, Ontario, Canada, August, 2001, pp. 488–491
26. Neamen, D.A.: Semiconductor Physics and Devices: Basic Principles. McGraw-Hill Education Press, 4th edn., pp. 156–191. New York (2017)
27. Li, G., Zhou, X., Li, X., et al: DC breakdown characteristics of XLPE/BNNS nanocomposites considering BN nanosheet concentration, space charge and temperature. High Volt. 5(3), 280–286 (2020)
28. Babu, M., Sarathi, R., Vasa, N., et al: Investigation on space charge and charge trap characteristics of gamma-irradiated epoxy micro–nano composites, High Volt. 5(2), 191–201 (2020)
29. Murakami, Y., Nemoto, M., Okuzumi, S., et al.: DC conduction and electrical breakdown of MgO/LDPE nanocomposite. IEEE Trans. Dielectr. Electr. Insul. 15(1), 33–39 (2008)
30. Markus, J., Anette, J., Villgot, E., et al.: High electron affinity: A guiding criterion for voltage stabilizer design. J. Phys Mater. Chem. A, 3(14), 7273–7286 (2015)

How to cite this article: Zhu, X., et al.: Mobility-limited charge injection in cross-linked polyethylene under extra high electric field. High Volt. 6(5), 782–792 (2021). https://doi.org/10.1049/hve2.12039